

Advances in energetic particle physics with Solar Orbiter

Robert F. Wimmer-Schweingruber,^{a,*} Alexander Kollhoff,^a Daniel Pacheco,^a Liu Yang,^a Javier Rodríguez-Pacheco,^b Raul Gómez-Herrero,^b Glenn M. Mason,^c Lars Berger,^a Patrick Kühl,^a Stephan I. Böttcher,^a Bernd Heber,^a Zigong Xu,^a Robert Allen,^c Angels Aran,^d Radoslav Bucik,^e Linghua Wang,^f Francisco Espinosa Lara,^b Ignacio Cernuda,^b Manuel Prieto,^b George C. Ho,^c Sandra Eldrum^a and Sebastian Fleth^a

^a*Inst. of Exp. & Appl. Phys., Kiel University,
Leibnizstr. 11, 24118 Kiel, Germany*

^b*Space Research Group, Universidad de Alcalá,
28805 Alcalá de Henares, Spain*

^c*Johns Hopkins University Applied Physics Laboratory,
Laurel, MD, USA*

^d*Departament de Física Quàntica i Astrofísica, Institut de Ciències del Cosmos (ICCUB), Universitat de
Barcelona (UB-IEEC),
Barcelona, Spain*

^e*Southwest Research Institute,
6220 Culebra Road, San Antonio, TX 78238, USA*

^f*School of Earth and Space Sciences, Peking University,
Beijing, 100871, People's Republic of China*

*E-mail: wimmer@physik.uni-kiel.de, kollhoff@physik.uni-kiel.de,
pacheco@physik.uni-kiel.de, yang@physik.uni-kiel.de, fsrodriguez@uah.es,
raul.gomez@uah.es, glenn.mason@jhuapl.edu, berger@physik.uni-kiel.de,
kuehl@physik.uni-kiel.de, boettcher@physik.uni-kiel.de,
heber@physik.uni-kiel.de, xu@physik.uni-kiel.de, Robert.Allen@jhuapl.edu,
angels.aran@fqa.ub.edu, radoslav.bucik@swri.org, wanglh@pku.edu.cn,
francisco.espinosal@uah.es, ignacio.cernuda@uah.es, manuel.prieto@uah.es,
george.ho@jhuapl.edu, eldrum@physik.uni-kiel.de, fleth@physik.uni-kiel.de*

*Speaker

The Sun drives a supersonic wind which inflates a giant plasma bubble in our very local interstellar neighborhood, the heliosphere. Its boundaries and the turbulent magnetic field shield the solar system from much of the interstellar medium as well as the low-energy portion of galactic cosmic rays (GCRs) which are accelerated primarily by super-nova-driven shocks in our galaxy. The heliosphere is bathed in an extremely variable background of energetic ions and electrons which originate from a number of sources. Solar energetic particles (SEPs) are accelerated in the vicinity of the Sun, whereas shocks driven by solar disturbances are observed to accelerate energetic storm particles (ESPs). Moreover, a dilute population with a distinct composition forms the anomalous cosmic rays (ACRs) which are of a mixed interstellar-heliospheric origin. Particles are also accelerated at planetary bow shocks. In February 2020, the European Space Agency (ESA) launched Solar Orbiter, a science mission to answer the question how the Sun creates and controls the heliosphere. Its orbit brings it within 0.3 astronomical units (au) from the Sun and will also reach moderately high solar latitudes to allow to understand why solar activity changes with time. The spacecraft carries instruments which observe the Sun and its surrounding remotely, others that measure the local environment, and some can track solar disturbances as they travel away from the Sun. The Energetic Particle Detector (EPD) on Solar Orbiter measures suprathermal and energetic particles in the energy range from a few keV up to (near-) relativistic energies (tens of MeV for electrons and about > 100 MeV/nuc for ions). Together with the other sophisticated instruments on Solar Orbiter it is designed to unravel how solar eruptions produce energetic particle radiation that fills the heliosphere. Since launch, EPD has made several advances about GCRs, SEPs, ACRs, ESPs, and the particles around the Venusian magnetosphere.

1. Introduction

Our Sun emits a supersonic solar wind which shapes the heliosphere, a giant plasma bubble which shields the solar system from interstellar space. The interaction of the solar wind with the interstellar medium leads to the formation of a termination shock where the solar wind turns subsonic at around 95 astronomical units (au) [1, 2] in the approximate upstream direction. Beyond that the now subsonic solar wind flows around the heliosphere. Because it (and a substantial part of the very local interstellar medium (VLISM)) is a magnetized plasma, it does not mix with the surrounding VLISM; the resulting boundary layer between solar and interstellar medium is commonly referred to as the heliopause.

In the inner heliosphere, the solar wind is highly non-thermal and characterized by strong suprathermal tails. It is also not the only particle population in the heliosphere. Galactic cosmic rays (GCRs) diffuse into the heliosphere, solar energetic particles are accelerated close to the Sun, interstellar neutrals (atoms) flow into the heliosphere where they are ionized and picked up by the solar wind to form so-called interstellar pickup ions [3] which are re-accelerated in the heliosheath to form anomalous cosmic rays (ACRs, [4–6]), particles are accelerated at interplanetary shocks or bow shocks of (magnetized) planets [7]. These various particle populations are accelerated by different processes (shocks, reconnection, turbulence) and at different locations. Their relative abundance / intensity is largely determined by solar activity which in turn is affected on many different time scales. The longest (non-solar) time scale must be given by changes in the galactic neighborhood and is not likely to be accessible to modern measurements [8] while changes in the more local neighborhood may have left imprints in terrestrial archives [9]. These can also be used to reconstruct long-term solar activity, on time scales of millennia [10, 11].

As is well known, the Sun undergoes an activity cycle which is driven by the solar dynamo [11]. We have illustrated this in Fig. 1 which shows four energy intensity (differential flux) spectra averaged over a Bartels rotation as dotted, dashed, solid, and dash-dotted lines. The upper panel shows sunspot number (Source: WDC-SILSO, Royal Observatory of Belgium, Brussels) which is a good indicator for solar activity as a function of time. The bottom panel shows the oxygen fluence accumulated over the four Bartels rotations indicated by vertical lines in the upper panel and in the title of the Figure. The line styles in the lower panel corresponds to those in the upper panel. Particle data were taken from three instruments on NASA’s Advanced Composition Explorer (ACE, [12]), the Ultra-Low-Energy Isotope Spectrometer (ULEIS, [13]) the Solar Isotope Spectrometer (SIS, [14]), and the Cosmic-Ray Isotope Spectrometer (CRIS, [15]). ACE/CRIS data for Bartels rotation 2001.830 (dotted line) are discussed in the following paragraph.

Fig. 1 also shows the highest and lowest particle fluences observed in the course of the ACE mission and illustrates the enormous variability of particle fluxes which is bounded by the shaded area. It covers a dynamic range of about seven orders of magnitude even when averaged over a Bartels rotation. Because of a malfunction of the second time-of-flight (ToF) measurement in the ULEIS instrument, fluxes at the highest energies covered by ULEIS during quiet times are affected by instrumental noise. The measured values are plotted as a line plot with a “+” symbol marking the values given by the ACE Science Center. Because we know that these values are not correct, we have also plotted a logarithmic interpolation between the lowest-energy SIS data point and the ULEIS data point with the highest energy which is not affected by this background (around 1 MeV/nuc).

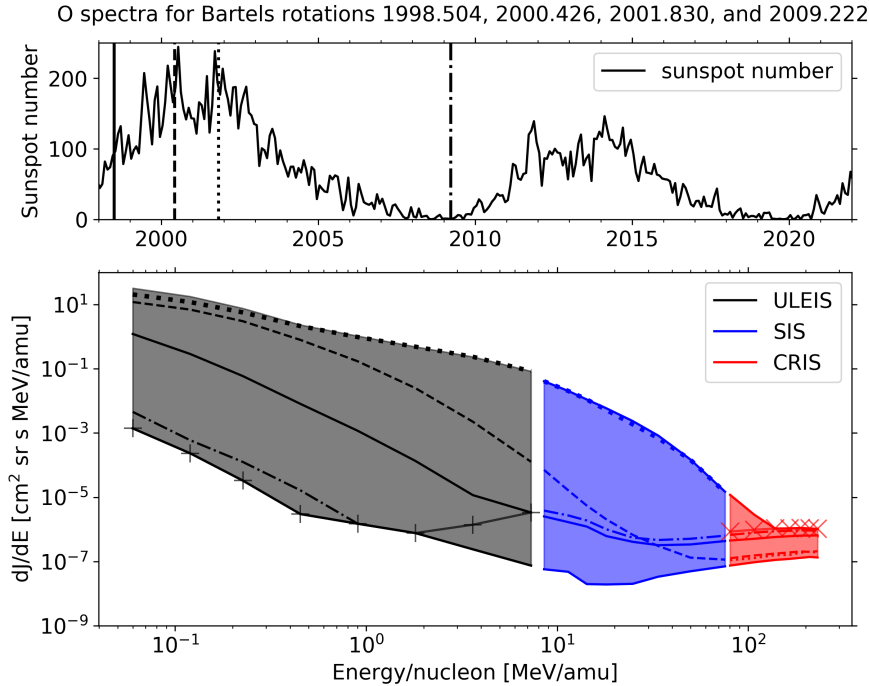


Figure 1: Oxygen fluence spectra accumulated over the time periods indicated by vertical lines in the upper panel (decimal years 1998.504, 2000.426, 2001.830, and 2009.222). Line styles in the lower panel indicate the Bartels rotation of the observation as indicated in the upper panel. Colors indicate different instruments on the ACE spacecraft as discussed in the text. The shaded region shows the envelope of the variability of the Bartels-rotation-averaged O particle fluences from 1998 – 2022. See text for an explanation of the “x” and “+” symbols.

The CRIS instrument on ACE was not designed to measure high fluxes during solar particle events but to provide accurate measurements of the quiet-time galactic cosmic rays. It saturates during high-flux time periods¹ which is seen by the measured data points which are also shown as a line plot with an “x” symbol marking. To establish a likely envelope, shown as the solid line bounding the shaded region, we have used a fluence of 0.8 times the highest-energy SIS data point and 0.8 times the square root of that value multiplied by the second-lowest CRIS fluence value. This is also the reason for the “missing” CRIS data in Fig. 1.

This paper discusses some of the advances in understanding the reasons of the enormous variability of energetic particles in the heliosphere just presented. We briefly discuss the joint ESA/NASA Solar Orbiter mission to the inner heliosphere in Sec. 2 and present a high-level summary the EPD instrument suite in Sec. 3. We discuss a sample of first results from EPD in Sec. 4 and conclude in Sec.5.

¹Dr. R. Leske, Caltech, private communication, 2022. See also the caveat at https://izw1.caltech.edu/ACE/ASC/level2/cris_l2desc.html which states that “Time periods during which solar activity is high are not covered by CRIS, since the instrument was not designed to operate during such conditions.”

2. Solar Orbiter

Solar Orbiter is a collaborative mission between ESA and NASA and was launched from Cape Canaveral on February 10, 2020 at 04:03 UTC. Its objective is to answer how the Sun creates and controls the Heliosphere – and why solar activity changes with time [16]. Solar Orbiter will answer this with its unique orbit design that brings it as close as 0.28 au to the Sun and with its scientific payload of six remote-sensing and four in situ instruments. Many of the instruments have multiple sensors. The payload allows to correlate measurements of the solar disk and atmosphere with in situ measurements and thus link the Sun to the heliosphere. Furthermore, its orbit will ultimately reach to significant elevation angles out of the ecliptic plane (up to 33°) and thus allow the first observations of the polar regions which are important to understand the solar dynamo. The planned mission duration is seven years with sufficient consumables for an extension by three years.

2.1 Top-Level Science Questions

The over-arching science objective is broken down into the four top-level science questions summarized in the following paragraphs.

2.1.1 What drives the solar wind and where does the coronal magnetic field originate?

It is currently still not fully understood how the solar corona is heated to temperatures greater than 1 MK. While we are currently confident that the fast solar wind stems from large, magnetically open coronal regions (coronal holes), the origin of the slow solar wind is still under debate. The most promising models for coronal heating rely on transferring energy from convective motion in the photosphere to the coronal magnetic field which then dissipates this energy through different processes. See, e.g., [17] for a recent review.

2.1.2 How do solar transients drive heliospheric variability?

Our active Sun drives various transient phenomena such as solar flares, coronal mass ejection (CMEs), eruptive prominences, or shocks in the corona and/or interplanetary space. These affect not only the solar wind as it moves from Sun to heliosphere, but can also affect planets and other bodies in the solar system. They are important drivers of what is called space weather which is also important in other (exo-) planetary systems, especially around active stars. Solar Orbiter's payload allows us to trace solar disturbances from the corona to the inner heliosphere; together with measurements from other spacecraft this extends our knowledge of their propagation to even larger distances [18, 19].

2.1.3 How do solar eruptions produce energetic particle radiation that fills the heliosphere?

The Sun occasionally accelerates ions and electrons to relativistic energies where the particles travel at nearly the speed of light. In some cases, ions have enough energy to penetrate the Earth's magnetosphere and part of its atmosphere and can be registered by neutron monitors as so-called ground-level events (GLEs, see [11] for a review). There are many more smaller solar energetic particle (SEP) events which typically don't reach such high energies but can still affect, e.g., space hardware. SEPs are also an important agent of space weathering, the process of slow surface alterations of airless bodies. Solar Orbiter will link eruptive processes in the low solar corona

through the corona and into the heliosphere by combining information from all its instruments. [20] provide a review of our understanding and current issues.

2.1.4 How does the solar dynamo work and drive connections between the Sun and heliosphere?

The solar magnetic field underlies most of the phenomena that are investigated by Solar Orbiter. It is the ultimate agent responsible for the heating of the corona, for the acceleration of the solar wind and SEPs, and for driving solar transients. The global magnetic field is generated by the dynamo process [21] in the solar interior. Despite significant advances in understanding it, we currently miss helioseismological observations of the polar regions that are crucial to understand the global circulation of the convective motions that drive the dynamo. See, e.g., [22] for a review of current issues.

2.2 Science Payload

The 1720 kg and 2.5 m × 3.1 m × 2.7 m Solar Orbiter spacecraft carries a payload of 10 scientific instruments with a total mass of 209 kg. The spacecraft is three-axis stabilized and protected from the intense solar heat around perihelion by a sophisticated heat shield [23]. The payload is often divided into two groups, remote-sensing instruments and instruments measuring in situ [16]. The spacecraft and payload are shown in Fig. 2. To reduce the influence of stray electromagnetic fields on the sensitive solar wind electron instrument (SWA, [24]), magnetometer (MAG, [25]), and radio plasma wave instrument (RPW, [26]) these instruments are mounted on a boom behind the spacecraft, in its shadow. The energetic particle detector (EPD, [27, 28]) has four sensors that are located close to three corners in the rear of the spacecraft, whereas the proton-alpha and heavy ion sensors (PAS and HIS, both part of SWA, [24]) are close to the heat shield to measure the solar wind which flows approximately radially away from the Sun. The radio plasma wave instrument also has sensors on three antennae that extend away from the spacecraft. Five of the six remote-sensing instruments are mounted inside the spacecraft and have closeable doors in the heat shield. The Extreme Ultraviolet Imager (EUI, [29]) combines three telescopes that image solar atmospheric layers from the solar chromosphere into the corona. The visible light and UV coronagraph (Metis, [30]) has an external occulter and provides visible light (580 – 640 nm) and UV images of the solar corona. The Polarimetric and Helioseismic Imager (SO/PHI, [31]) consists of two telescopes that provide high-resolution and full-disc maps of the photospheric vector magnetic field and line-of-sight velocity as well as of the continuum intensity. The Spectral Imaging of the Coronal Environment (SPICE, [32]) provides high-resolution spectral images at extreme ultraviolet wavelengths. Finally, the Solar Orbiter Heliospheric Imager (SoloHI, [33]) has a wide field of view that images the inner heliosphere in visible photospheric light scattered by solar wind electrons (and interplanetary dust) and is mounted on the wake side of the spacecraft, in the vicinity of one of the EPD sensors. Thus Solar Orbiter has a very sophisticated payload which has been designed and optimized to solve the questions discussed in Sec. 2.1.

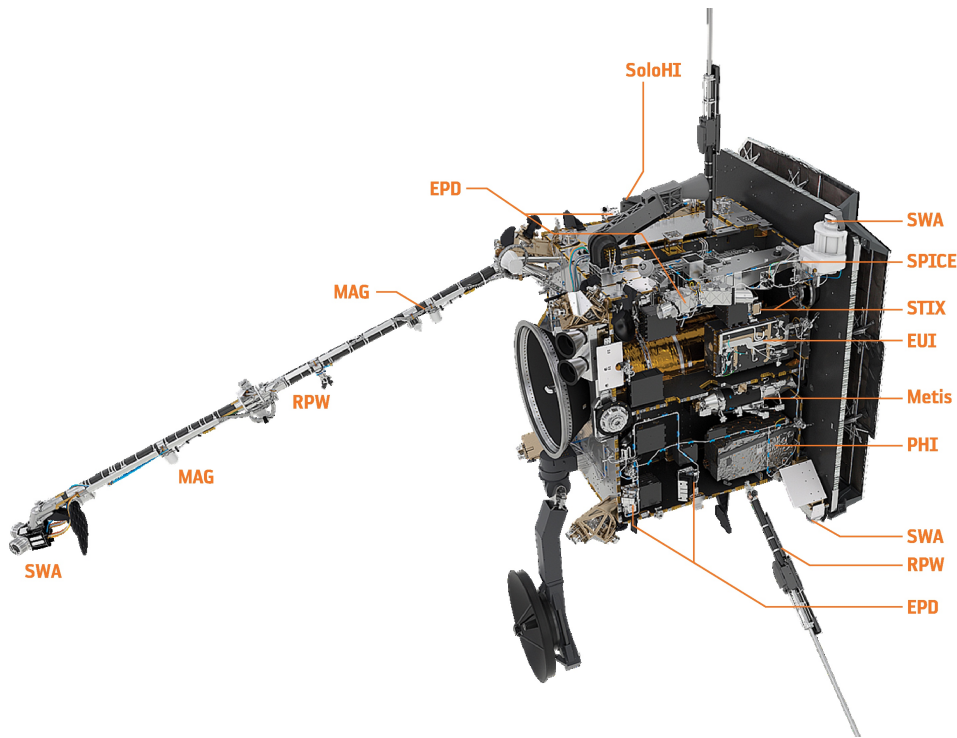


Figure 2: The Solar Orbiter spacecraft accommodates the ten scientific instruments which are indicated by their acronyms. Multiple mentions of the same acronym refer to multiple sensors of that instrument. The heat shield at the front (right) of the spacecraft protects it from the intense solar heat around perihelion. See text for more information. Credit: [16], reproduced with permission © ESO.

3. The Solar Orbiter Energetic Particle Detector

The Energetic Particle Detector (EPD) suite of sensors is described in [27] with important updates provided by [28]. It consists of four sensors which we describe briefly in ascending energy range, as given in the overview Fig. 3. The supra-thermal electron and proton (STEP) sensor measures electrons between few keV to beyond 80 keV and ions from several keV to ~ 100 keV in 15 viewing directions at a cadence of one second. This is achieved with two sensor heads which point in the same direction and use a pin-hole design and a 3×5 pixel solid-state detector. One sensor head uses a strong permanent-magnet system to deflect electrons and measures only ions, the other is field free and measures ions and electrons. Determining the difference between the two measurements then provides the electron flux. Note that, despite its name, STEP can not discriminate protons from heavier ions.

The two dual-ended electron-proton telescope (EPT) sensors share their electronic boxes with the high-energy telescope (HET). The two EPTs measure electrons and protons (ions) from 25 keV to ~ 475 keV (electrons) or ~ 6.4 MeV protons. Similar to STEP, in this energy range EPT can not discriminate protons from heavier ions, and measures at a cadence of one second. Electrons and protons (ions) are discriminated using the magnet-foil technique [27]. The two dual-ended telescopes provide electron and proton (ion) measurements in four viewing directions, one approximately along the nominal Parker spiral angle, the other anti-parallel to this direction, the

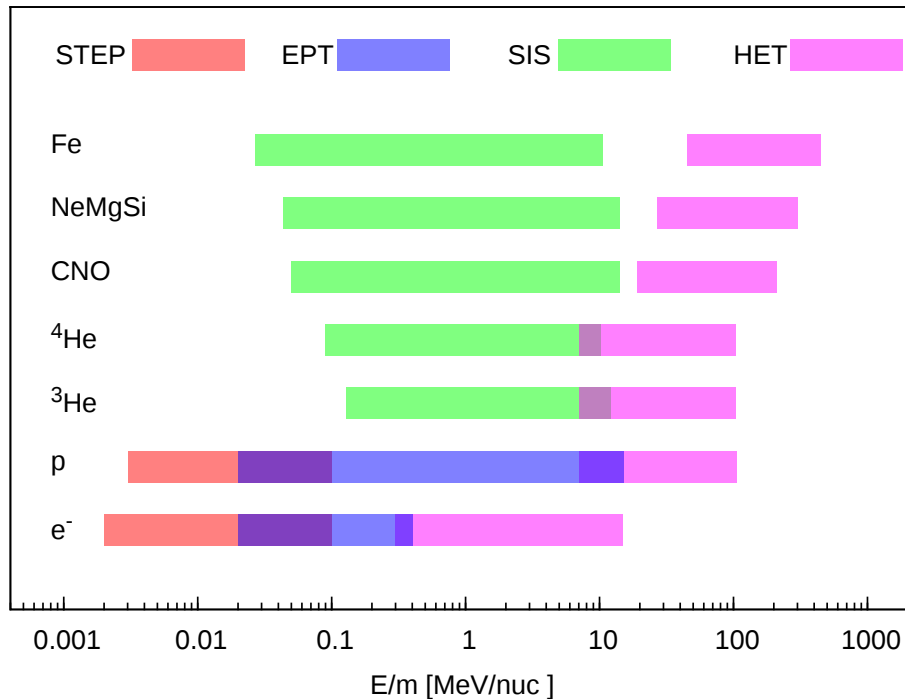


Figure 3: The Energetic Particle Detector (EPD) on Solar Orbiter measures electrons from a few keV up to relativistic energies exceeding 20 MeV. Ions are measured from few keV up to species-dependent energy or energy per mass > 100 MeV/nuc. The different sensors have overlapping energy ranges. Adapted from [27].

other two are perpendicular, approximately in the polar directions.

The supra-thermal ion spectrograph (SIS) measures the elemental composition of suprathermal ions and the isotopic composition of helium. It has two nearly oppositely pointing telescopes that allow it to determine first-order anisotropy and has a maximum (typical) cadence of 3 (30) seconds. It uses multiple time-of-flight measurements as well as the measurement of total residual energy and because of these multiple coincidence measurements has a very low background that allows to measure the ionic composition during quiet time periods.

The high-energy telescope (HET) measures electrons between ~ 0.3 –30 MeV and ions between ~ 7 –100 MeV/nuc, but this energy range depends strongly on the ion and reaches higher values for heavier elements. It determines differential fluxes of individual elements and can discriminate the helium isotopes for which there is also an energy overlap with SIS. It shares the electronics box with EPT and points in the same four directions as EPT, but with a larger field of view. HET also measures at a cadence up to one second.

4. First Results

4.1 Overview

The enormous variability in the flux of heliospheric energetic particles is also seen by Solar Orbiter. The four panels in Fig. 4 show particle measurements for 54–101 keV electrons (pointing

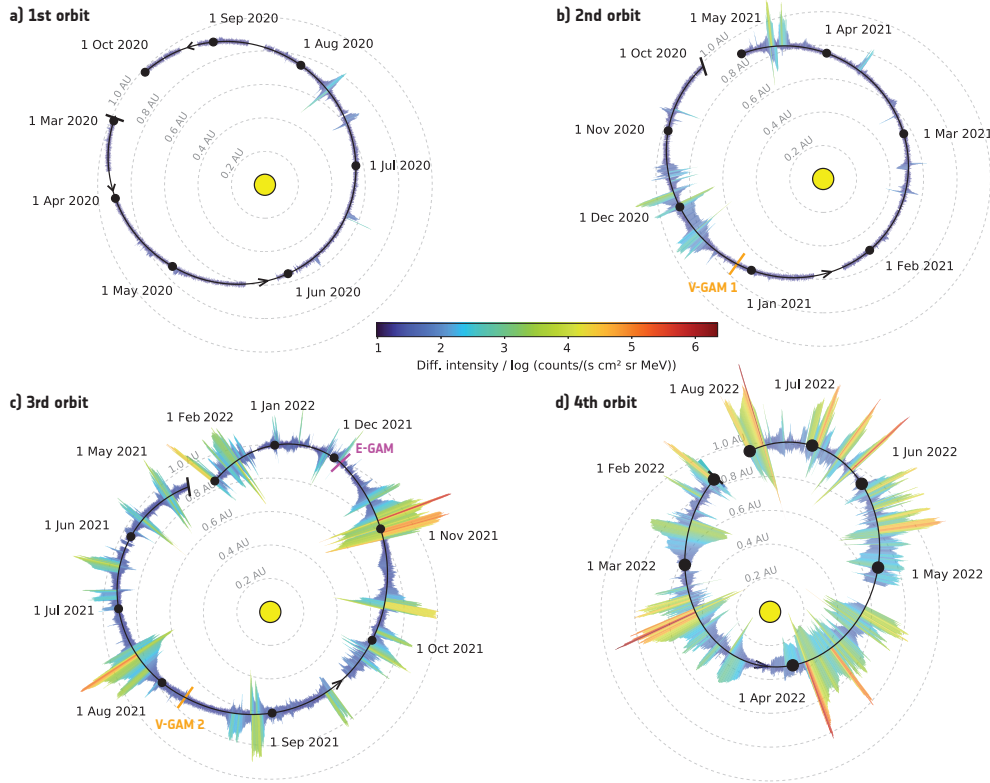


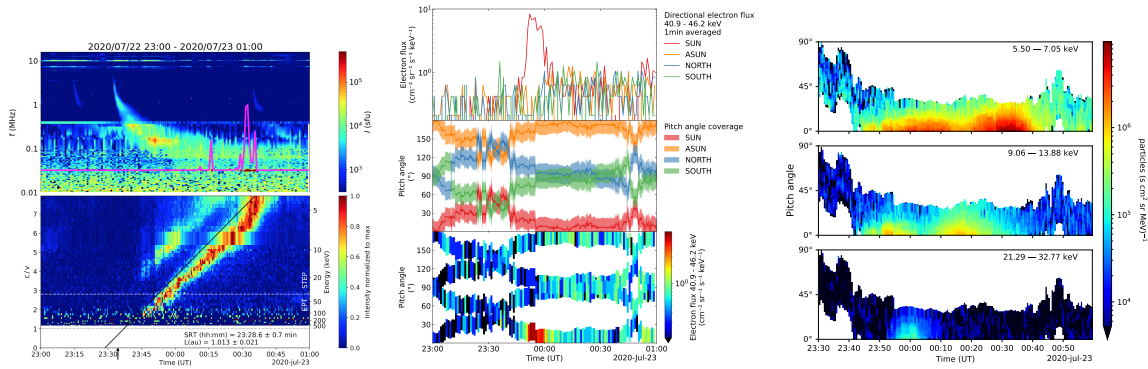
Figure 4: Evolution of the differential fluxes of 54–101 keV electrons (pointing inwards) and 124–218 keV ions (outwards) from Solar Orbiter’s first (a, March through September 2020), second, (b, October 2020 through April 2021), third (c, May 2021 through January 2022), to fourth (d, February through July 2022) orbit. Differential fluxes are also color coded according to the color bar in the middle of the figure. The figure illustrates the dramatic increase of solar activity between 2020 and 2022. The seemingly strange shape of the third orbit is a consequence of the Gravity Assist Maneuvers (GAMs, as indicated) in 2021. Orbits are drawn in the mean ecliptic and equinox of J2000 (ECLIPJ2000) reference frame.

inwards) and 124–218 keV ions (outwards) for the first four orbits of the mission. Intensities are color coded and the extent of the excursion from the orbit is also a measure of the intensity. The ellipticity of the orbit was changed by two Venus and one Earth Gravity Assist Maneuvers (GAMs) that are also marked in the figure. A total of one EGAM and seven VGAMs will ultimately change Solar Orbiter’s orbital inclination to $\sim 34^\circ$ to enable remote observations of the polar regions. In the following we discuss some of the first science results of the mission which were also reported in a special issue of *Astronomy & Astrophysics* on first results from Solar Orbiter (<https://www.aanda.org/component/toc/?task=topic&id=1340>).

4.2 Near-relativistic electrons

One of the aims of Solar Orbiter is to explore the physical processes that link the Sun and the heliosphere². Near-relativistic (n-r) electrons are accelerated in association with type III radio bursts

²This may be considered part of how the Sun creates and controls the heliosphere.



(a) Upper panel: RPW dynamic spectrum, the magenta line indicates the spectral flux at the local plasma frequency, where the peaks indicate locally generated Langmuir waves. Lower panel: Electron c/v versus time plot. The color scale corresponds to the particle intensity, normalized to the maximum value for each energy (speed) channel.

(b) Time evolution of directional electron intensity measurements during the July 22 event. From top to bottom: 1) 40.9 - 46.2 keV electron intensities observed by the four EPD apertures; 2) pitch-angle coverage corresponding to each aperture; and 3) pitch angle distribution with color-coded intensity for the same energy range shown in the first panel.

(c) Electron pitch-angle distributions observed by STEP at three different energy bands (5.5 - 7.05 keV, 9.06 - 13.88 keV, and 21.29 - 32.77 keV) during the July 22 event. The time scale is the same as the ones used in Figs. 5a and 5b, but the Y-axis only covers the interval 0-90°. Note that higher-energy electrons arrive earlier than lower-energy electrons.

Figure 5: Detailed analysis of the 22 July 2020 event. Credit [35], reproduced with permission, © ESO.

and with ^3He -rich ion emissions [34]. Because of their very high speed n-r electrons are excellent tracers of the sources of SEPs at the Sun, but also of the magnetic connectivity. Nevertheless, several puzzles have proven impervious to solutions so far [35]: The close temporal association of n-r electrons observed by Helios with type III radio bursts and hard X-rays is not seen with instruments stationed farther away. The energy spectra of electrons observed in space do not show a simple relation to energy spectra derived from solar hard X-ray emission [36]. Moreover, n-r electrons are frequently detected at widely separated spacecraft (s/c) which is not understood. These puzzling observations indicate that we do not understand the acceleration and transport processes in the corona and heliosphere. EPD and RPW Observations in July 2020 between 0.61 and 0.69 au reported by [35] show the potential of Solar Orbiter to solve these questions. Those authors found five n-r electron events (July 11, 19, 20, 21, and 22, see also Fig. 4a) that were associated with type III radio bursts. Extreme ultra-violet (EUV) jets were observed by STEREO A and SDO for four of them, but only the 11 July n-r- electron event was also seen at an other spacecraft (Wind) which was separated by 107 degrees in longitude. EPD/SIS on Solar Orbiter measured strongly enhanced ^3He [37] preceding the July 22 event which was also the most anisotropic of all. RPW on Solar Orbiter detected Langmuir waves in situ for this July 22 event [35], and imaging by STEREO A indicates that the jet was confined to non-radial coronal magnetic field lines which may explain the large angular distance between Solar Orbiter's nominal magnetic foot point and the flaring site. Figure 5 shows the observations for this event.

When the interplanetary magnetic field is favorably oriented with respect to STEP, its pin-hole design allow to measure the pitch-angle distribution of electron and ions with very high resolution. An example is shown in [28] who investigated the 10 - 11 December 2020 particle event. Their

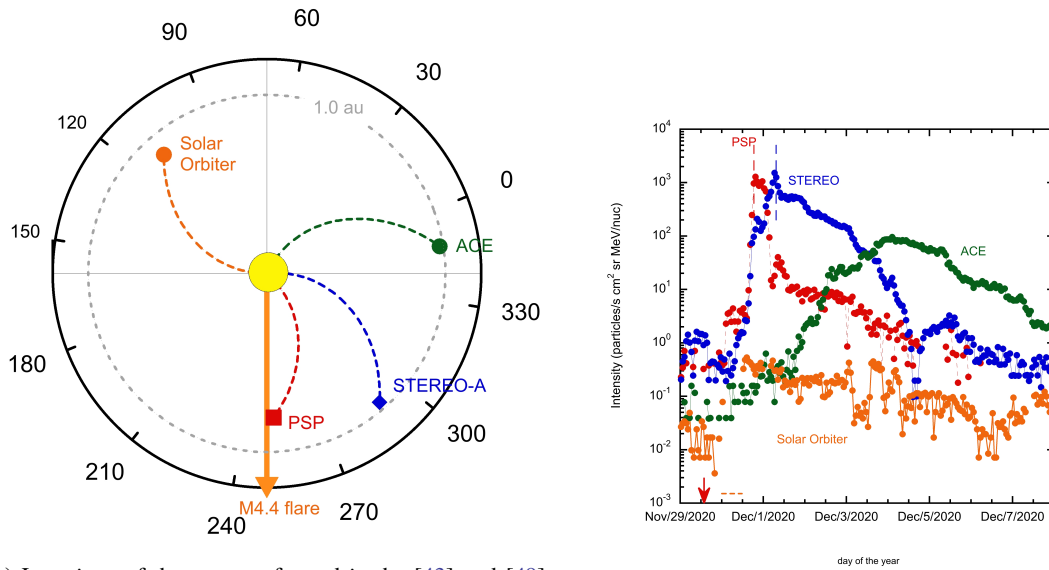
Fig. 3 shows that at the onset of this event, electrons were strongly beamed with a $1/e$ width of ~ 13 degrees, despite Solar Orbiter being at a heliocentric distance of 0.82 au. This measurement is consistent with the observations by [38], but those measurement could only give an upper limit of 15° for low-energy electrons (10 - 40 keV). These observations pose strong limits on the scattering of electrons in the interplanetary magnetic field, i.e., on the wave-particle interactions en route from the Sun to 0.82 au (and out to 1 au [38]). Note that previous instrumentation did not usually have such high angular resolution and the very small scattering in this event would not have been seen in this clarity because lower angular resolution would have smeared out this narrow beam.

4.3 ^3He -rich events

As can be seen by comparing Fig. 4a with Figs. 4b - 4d, solar activity in this first orbit was low. This offered an excellent and nearly background-free opportunity (but see Sec. 4.4) to study small ^3He -rich events. Such events are associated with soft X-ray emission, type III radio bursts and energetic particles, and often with enhanced heavy ion fluxes. [37] studied the composition of suprathermal particles in three events which can be clearly seen in Fig. 4a (18 June, 11 & 20 July) and two (5 August & 17 September) which were so small that they barely show up in this overview plot. All exhibited elevated $^3\text{He}/^4\text{He}$ ratios and all but the 11 July event had enhanced > 35 keV electron fluxes. The 20 July event was notable because of its high anisotropies (Sun/anti-Sun ~ 5) and because its intensity was large enough to measure its composition which was enriched in heavy ions as is typical of impulsive, ^3He -rich events. As can be seen in Fig. 5 there were two electron injections for the 22 July 2020 event³ which are associated with type III radio bursts. Interestingly, during the period reported by [37] ACE observed no impulsive ion events at 1 au. This illustrates an important advantage of Solar Orbiter: By going closer to the Sun it becomes increasingly easier to disentangle individual events and transport effects which often smear out the properties of the events by the time the particles reach one au. By approaching close to the Sun it will be possible to determine whether individual type III radio bursts lead to individual ^3He -rich ion injections which can not be ascertained at one au because of transport effect. If type III radio bursts and ^3He ion injections are indeed closely associated, then that would indicate that ions and electrons are accelerated in the same location, which to date is unclear.

Recurrent ^3He -rich SEP events have been found to originate from active regions at the boundary of low-latitude coronal holes (e.g., [39]), but only a few ^3He -rich SEPs have been reported which were associated with sunspot jets [40, 41]. None of them report recurrent ion injection. [42] report a configuration with two large and complex nearby active regions which may have been responsible for five recurrent particle injections observed by EPD between 17 and 20 November 2020. All of them showed enhanced $^3\text{He}/^4\text{He}$ and Fe/O abundance ratios and several of them concurrent electron injections. [42] conjecture that there may be a long-lived interaction between the negative polarity of one active region and the positive polarity of the neighboring active region, leading to the magnetic reconnection which drives the acceleration of ions and electrons. The two active regions were also located such that they produced a longitudinally extended source ($\sim 40^\circ$) which may explain the multiple injections from the same source region.

³See also Sec. 4.2 and [35].



(a) Locations of the spacecraft used in the [43] and [49] studies in Carrington longitude and heliocentric distance during the 29 November 2020 flare. The dashed lines indicate nominal Parker spirals for a solar wind speed of 400 km/s.

(b) Hourly intensities of 273 keV/nuc ^4He at Solar Orbiter, PSP, STEREO-A, and ACE. The downward-pointing red arrow shows the time of the flare, dashed vertical lines for PSP and STEREO-A show the time of passage of the shock.

Figure 6: Credit [43], reproduced with permission, © ESO.

4.4 Heavy Ions

The EPD/SIS instrument measures suprathermal ions in the energy range $\sim 0.01 - 20$ MeV/nuc in 21 energy/nucleon bins and resolves the helium isotopes [27]. It measured the properties of heavy ions during the widespread 29 November 2020 solar particle event which is also discussed below in Sec. 4.6. [43] compare measurements at Solar Orbiter (at $r = 0.88$ au, $\varphi = 110^\circ$ Carrington longitude) with data from PSP ($r = 0.81$ au, $\varphi = 252^\circ$), STEREO-A ($r = 0.96$ au, $\varphi = 290^\circ$), and ACE ($r = 0.98$ au, $\varphi = 348^\circ$), as shown in Fig. 6a. Figure 6b shows hourly intensities at each spacecraft. The rise times of intensities are typical of low energy ions when considering the longitudinal separations of the spacecraft from the flare location ($\varphi = 249^\circ$). The measurements reported by [43] show spectral breaks which are comparable to previous results. The authors fitted band functions [44] to the observed spectra at Solar Orbiter and found that the high-energy power-law index for this event was considerably larger than the average one found by [45] who surveyed 64 well-connected western hemisphere SEPs with no local Interplanetary (IP) Shock or Energetic Storm Particle (ESP) component. At PSP and STEREO-A the intensity profiles were likely strongly affected by the shock [46]. The PSP and ACE heavy ion abundances (normalized to O) are about two times lower than survey averages for masses > 40 nuc, but depend strongly on the energy per nuc at which this is evaluated. At energies < 200 keV/nuc PSP and STEREO Fe/O ratios are approximately twice as large as at ACE and Solar Orbiter, which were further away in longitude from the event site. This is consistent with the differences seen in Fe/O ratios of large solar particle events versus events dominated by intensities near an interplanetary shock passage [47, 48]. No enhancement of $^3\text{He}/^4\text{He}$ was observed for this event.

The quiet first orbit of Solar Orbiter (see Fig. 4a) provided an excellent opportunity to investigate the origin of the quiet-time population of energetic particles in the heliosphere. During quiet-times (i.e., during times when transient solar particle events, interplanetary shocks, and other activity are absent) low energy ion spectra in the interplanetary medium near 1 au are formed by galactic cosmic rays (GCRs), anomalous cosmic rays (ACRs), and a "turn-up" spectrum below a few MeV/nucleon that increases with decreasing energy. It has been a long-standing question how important the so-called "remnant-flare" population is for supplying the "turn-up" portion of the spectrum (at low energies, beneath about 1 MeV/nuc). Solar Orbiter will make progress on this question because of its ultimately inclined orbit and the broad range of radial distances which it covers. [50] studied "quiet times" by removing time periods with obvious activity in hourly He intensity averages around 270 keV/nuc, resulting in 2386 hours worth of data. Figure 7 shows quiet-time spectra from SIS (filled circles) and HET (filled diamonds), augmented by some data from ACE (open circles). Comparison of these spectra with similar ones from SAMPEX [51] shows intriguing differences, especially the location of the maximum of the ACR O component which is prominently visible at lower energies in 2020 than in the SAMPEX data (which are from 1992/1993). The "turn-up" spectra at lower energies are consistent with impulsive SEP material, especially because of the high $^3\text{He}/^4\text{He}$ ratio which at $\sim 20\%$ is considerably higher than previous results. This could be because Solar Orbiter measured closer to the Sun where SEP intensities are higher and the contribution from co-rotating interaction regions (CIRs) is lower ([52], see also Sec. 4.7). [50] also investigated a 192-hour "super-quiet" period in which the proton spectrum extends to 1 MeV, but ^4He shows a sharp drop-off above 200 keV/nucleon. The difference between the H and ^4He drop-off energies may be a clue for the accelerating mechanism. Unfortunately, measurements of heavier ions are currently very limited statistically. We will need to wait for the Sun to return to its activity minimum again, before this question can be settled.

4.5 Radial Evolution of the Solar Wind Plasma

Turbulence is an essential ingredient in our understanding of the acceleration and transport of energetic particles. [53] used a radial alignment of PSP and Solar Orbiter to determine the radial evolution of solar wind turbulence from 0.1 to 1 au. They assumed ballistic propagation to identify two 1.5 hr intervals that provided measurements of the same plasma parcels traveling from 0.1 to 1 au. Their results show that the plasma evolves from a highly Alfvénic, less-developed turbulence state near the Sun, to fully developed and intermittent turbulence at 1 au. Their statistical analysis of the intervals at PSP and Solar Orbiter appears to show that turbulence evolves during solar wind expansion and that nonlinear interactions between Alfvén waves probably had not yet fully developed at 0.1 au, where the solar wind sampled by PSP is to a good approximation pristine. At Solar Orbiter, close to 1 au, the nonlinear interactions appeared to have formed a fully developed spectrum. Another explanation may be that the decrease of the Alfvénic fluctuations could have exposed the intermittent nature of the advected coherent structures. Furthermore, [54] used the first Solar Orbiter — Parker Solar Probe quadrature to track the evolution of solar wind from the extended corona to the inner heliosphere. They used the Metis coronagraph on Solar Orbiter to observe a plasma volume between 3.5 and 6.3 solar radii which was subsequently also sampled in situ by PSP. This measurement made it possible to link the local properties of the solar wind to the coronal source region from where it originated and to estimate the Alfvén radius during this fortuitous quadrature.

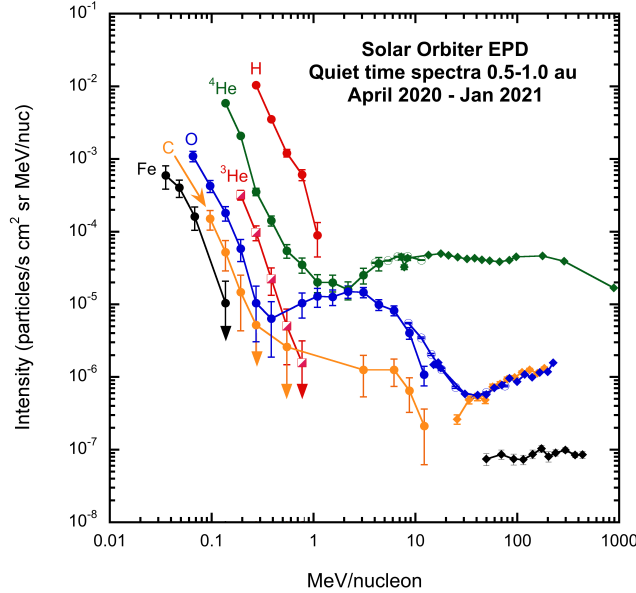


Figure 7: Quiet-time spectra measured by Solar Orbiter EPD/SIS (filled circles and half-filled squares), EPD/HET (filled diamonds), and ACE at 1 au (open circles). Downward pointing arrows signify one-count upper limits. Credit [50], reproduced with permission,

These studies were complemented by those of [55] who compared measurements in fast and slow wind with results of a nearly incompressible magneto-hydrodynamic (NI MHD) model to find good agreement. They interpreted this as a change of the ratio of 2D and slab energy as the angle between the mean solar wind flow and the mean magnetic field increases.

The expansion of CMEs is governed primarily by their intrinsic pressure and their speeds relative to the surrounding solar wind. When they drive strong shocks close to the Sun they are believed to be the main particle accelerator in gradual events (see, e.g., [20] for a recent review). Thus it is of great interest to understand the radial evolution of CMEs. The strong magnetic field shields part of the flux of (low-energy) GCRs so that the passage of CMEs can often be measured by detecting a depression in the GCR count rate (Forbush decrease, [56]). Solar Orbiter detected a CME-driven shock on April 19, 2020 at 05:07 [57] when it was upstream of Earth and BepiColombo was close to Earth, as can be seen in Fig. 8. This gave an excellent opportunity to observe a CME and the shock driven by it, as well as the particles accelerated by it at multiple locations. In addition, STEREO A observed the CME in approximate quadrature. EPD's HET has GCR counters which were implemented to detect Forbush decreases and [19] used a 3% Forbush decrease to detect the Earth-directed stealth CME that passed Solar Orbiter on April 19, 2020 and was also visible as a 2% Forbush decrease with the Cosmic Ray Telescope for the Effects of Radiation (CRaTER, [58]) on board the Lunar Reconnaissance Orbiter [59] and a 1% decrease in neutron monitor measurements. They found significant differences in the expansion behavior of the CME at the

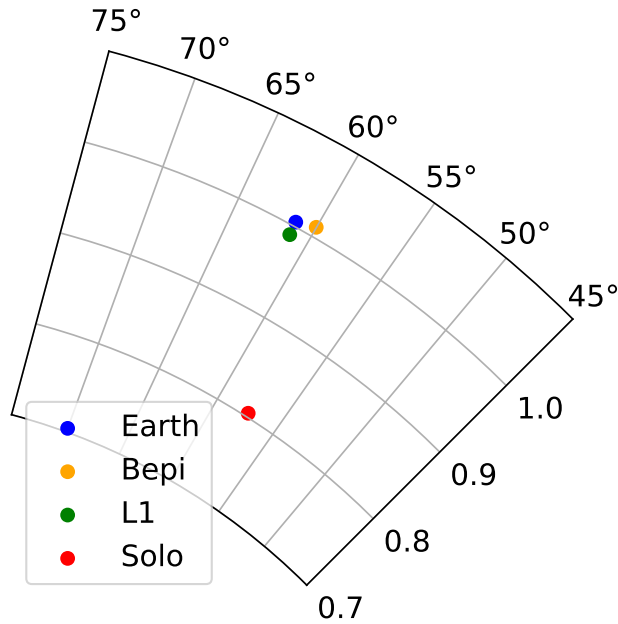


Figure 8: Positions of Earth (blue), BepiColombo (orange), Earth-Sun Lagrange point L1 (black), and Solar Orbiter (red) on 2020-04-20 00:00:00 in Carrington coordinates. The Sun would lie at $r = 0$ downwards towards the left.

two different locations. Because Solar Orbiter was located at 0.8 au from the Sun and upstream of the Earth at this time, they interpreted these differences as due to the influence of the following high speed solar wind stream. [60] found that this CME originated from a quiet Sun cavity with an extremely weak field. They attributed the strong magnetic field measured in situ as a consequence of the interaction of the ICME with its surrounding environment. The same CME was also studied by [61] who used the in situ observations of the CME at Solar Orbiter, Wind, and BepiColombo and the remote observations of the CME at STEREO-A. BepiColombo was also close to Earth at this time. This multi-spacecraft constellation made it possible to determine the global shape of the CME and its evolution as it propagated through the inner heliosphere. [61] found that the dependence of the maximum (mean) magnetic field strength decreased with heliocentric distance as $r^{-1.24 \pm 0.50}$ ($r^{-1.12 \pm 0.14}$), disagreeing with previous studies. Their detailed study of the axial and poloidal magnetic field strength dependencies led them to conclude that the CME expansion is probably neither self-similar nor cylindrically symmetric. [62] studied the turbulence and wave transmission at the shock driven by this ICME and found that, after the shock crossing, the magnetic field fluctuation power increases. In the vicinity of the shock, they observed right-hand polarized waves in the spacecraft frame and that the upstream wave signatures fall within a relatively broad and low frequency band, which might be attributed to low frequency MHD waves excited by the streaming particles. Together these observations imply that stealth CMEs require multi-wavelength and multi-viewpoint observations in order to confidently locate the source region and that their elusive signatures pose significant challenges to space weather forecasting.

4.6 Wide-spread events

Although the origin of solar eruptions which drive CMEs can often be very accurately located in the low corona, the CMEs they drive nevertheless often produce energetic particle radiation that fills the heliosphere. [49] investigated the first such event observed by Solar Orbiter on November 29, 2020. It is seen as an increase just before 1 Dec 2020 in Fig. 4b. This particle event was also observed by NASA’s Parker Solar Probe (PSP [63]), the Solar Terrestrial Relations Observatory (STEREO-A, [64]), and multiple spacecraft at Earth. The locations of the various spacecraft are given in Fig. 6a. The observations at multiple, wide-spread locations in the heliosphere imply that particles must have spread across more than 230° in longitude close to one au. [49] found that the onsets at the multiple locations exhibited delays which increased with increasing angular separation from the flare foot-point which could not be explained by the propagation time of the flare-driven EUV wave to the likely foot points of the multiple spacecraft. Moreover, they found anisotropic particle distributions at Solar Orbiter, STEREO, and Earth which appear to allow particle injection across a wide longitudinal range close to the Sun. The same event was also studied by [43] but with a focus on the differences in energy spectra of different elements at Solar Orbiter, PSP, STEREO-A, and ACE. Their observations make it possible to test, constrain, and refine models of particle acceleration and transport.

4.7 Corotating Interaction Regions (CIRs)

Because the solar wind is a magnetized plasma, different solar wind parcels do not mix (in the absence of magnetic reconnection). Thus, when fast solar wind catches up with slow wind, a so-called stream interaction region (SIR) forms in which pressure builds up and waves transport the information of the “obstacle” into the compressed fast and slow wind. Well beyond 1 au, these waves steepen into shock waves which are known to accelerate particles. During solar activity minimum, coronal holes generally last for several solar rotation periods and so-called co-rotating interaction regions form⁴. During its first orbit, Solar Orbiter observed six CIR structures [52], five of which were also observed at one au by the Ultra-Low Energy Isotope Spectrometer (ULEIS, [13]) on ACE. Because SIS was completing commissioning during the time period of the first CIR, this left four CIRs for which intensities and spectra could be compared at two different heliocentric distances. [52] found that ^4He spectral indices for 0.2 – 1 MeV/nuc at the two locations were similar, but their intensities were much lower at Solar Orbiter than at ACE. The similarities of the spectral indices suggested that energy-dependent modulation due to transport processes (i.e., the the spectral hardening of lower-energy ions as predicted by [66]) is not observed. [52] also compared the ratio of 226 – 320 keV/nuc ^4He ion intensities from SIS at 0.5 au normalized to those observed at 1 au by ULEIS and found that the relative intensity scaled with heliocentric distance very similarly to the 0.9 to 2.2 MeV H intensities reported by [67, 68]. This is remarkable because the same gradient is seen despite the different species and energies (and thus rigidities). More work with different elements, more CIRs, and different helio-latitudes will certainly shed light on transport properties of these suprathermal particles and the transport processes affecting them.

⁴The reader is referred to the excellent collection of reviews in [65] for an in-depth discussion of such interaction regions.

4.8 Observations of in situ acceleration at a developing stream interaction region

EPD on Solar Orbiter has also detected local acceleration of ions in a likely CIR at 0.52 au from the Sun [69]. The flux of accelerated ions was clearly anisotropic and flowing away from the Sun. This anisotropy was observed in the compressed fast wind region, but the compression was only weak, as would be assumed at these heliocentric distances. Moreover, particle intensities rose and peaked simultaneously in the different EPT energy channels. This led [69] to rule out that these particles had been accelerated by a distant region of the CIR and diffused inward, as discussed in the previous section 4.7. Therefore, [69] suggested that a local stochastic acceleration process was a more plausible mechanism to explain the observed sudden low-energy ion enhancement. CIRs generally only develop shocks well beyond 1 au, and particles accelerated by these shocks would have to diffuse inward and would therefore show a sunward anisotropy. These observations are similar to previous ones by [70] in compression regions at one au. [71] subsequently showed that that compression regions associated with CIRs at 1 AU with widths ~ 0.03 au can accelerate particles up to ~ 10 MeV and produce energy spectra which were remarkably similar to the observations of [70]. Thus the observation reported by [69] indicates that local stochastic acceleration is already active well within one au, at 0.52 au at SIRs that are only just beginning to form.

5. Summary and Conclusions

At the time of the launch of Solar Orbiter, solar activity was low which allowed us to study particle populations and their properties which are otherwise masked by solar activity. Examples include radial gradients of particles accelerated at CIRs [52] or spectra of anomalous oxygen and helium [50]. The first solar particle events were thus also isolated and free of remnant suprathermal particles from previous events. For example this allowed [69] to detect the small increase in locally accelerated particles at the only just forming SIR at 0.52 au. Because shocks had not yet formed there and anisotropies were anti-sunward, this observation suggested that these low-energy particles were accelerated in the compression region by a stochastic acceleration process.

With the addition of Solar Orbiter to the fleet of spacecraft operating in the inner heliosphere multi-spacecraft observations close to the Sun are starting to unveil some of the puzzles of particle acceleration. For example the evolution of the turbulent cascade from close to the Sun to one au was studied by [53, 54]. How this evolves across the inner heliosphere is key to understanding the transport of energetic particles and to limit scenarios to explain wide-spread events, such as that studied by [49]. This study also underlines the importance of using information from multiple instruments at the various locations. The combination of data from multiple spacecraft also enables to track the motion of coronal mass ejections through the heliosphere [19, 60–62]. These studies emphasized the importance of using information from multiple instruments on multiple spacecraft at multiple locations to understand the three-dimensional nature of the propagation of CMEs.

With its varying location in the inner heliosphere and excellent instrumentation, Solar Orbiter also opens new windows for the investigation of near-relativistic electrons [35], ^3He -rich events [42, 43], and detailed measurements of heavy-ion composition [43] which can be used as a sensitive indicator of acceleration mechanism.

Since the first year of operating Solar Orbiter it has become clear that its telemetry is much better than is was originally and conservatively estimated and so it was possible to considerably

increase the data transfer rate to ground. This has allowed EPD STEP, EPT, and HET to produce a wealth of data at a cadence on one second. The energy (and angular) resolution of EPT and STEP were also increased in the telemetry, thus allowing future studies of the micro-physical processes responsible for the energization of suprathermal and energetic particles in the heliosphere.

We have attempted to give an impression of the richness of observations offered by Solar Orbiter already during its commissioning phase when the in situ instruments were already measuring and the remote-sensing instruments were generally not yet active. Since then the remote-sensing payload has also been commissioned and new, exciting discoveries have been made. With its unique orbit, Solar Orbiter has also offered serendipitous science opportunities, such as the fly-bys of Venus [72–75] or the detection of the hitherto elusive nano-flares by the Extreme Ultraviolet Imager, EUVI, [76] which we have not even mentioned in this review.

Acknowledgments

Solar Orbiter is a space mission of international collaboration between ESA and NASA, operated by ESA. The Energetic Particle Detector was supported by the Spanish Ministerio de Ciencia, Innovación y Universidades under grants FEDER/MCIU – Agencia Estatal de Investigación/Projects ESP2015-68266-R, ESP2017-88436-R and PID2019-104863RB-I00/AEI/10.13039/501100011033. We thank the German Federal Ministry for Economic Affairs and Energy and the German Space Agency (Deutsches Zentrum für Luft- und Raumfahrt, e.V., (DLR)) for their unwavering support of STEP, EPT, and HET under grants numbers 50OT0901, 50OT1202, 50OT1702, and 50OT2002; and ESA for supporting the build of SIS under contract number SOL.ASTR.CON.00004, as well as the University of Kiel and the Land Schleswig-Holstein for their support of SIS. We thank NASA headquarters and the GSFC Solar Orbiter project office for support of SIS at APL under contract NNN06AA01C.

References

- [1] E.C. Stone, A.C. Cummings, F.B. McDonald, B.C. Heikkila, N. Lal and W.R. Webber, *Voyager 1 Explores the Termination Shock Region and the Heliosheath Beyond*, *Science* **309** (2005) 2017.
- [2] L.F. Burlaga, N.F. Ness, M.H. Acuña, R.P. Lepping, J.E.P. Connerney, E.C. Stone et al., *Crossing the Termination Shock into the Heliosheath: Magnetic Fields*, *Science* **309** (2005) 2027.
- [3] E. Möbius, D. Hovestadt, B. Klecker, M. Scholer, G. Gloeckler and F.M. Ipavich, *Direct observation of He⁺ pick-up ions of interstellar origin in the solar wind*, *Nature* **318** (1985) 426 .
- [4] M. Garcia-Munoz, G.M. Mason and J.A. Simpson, *A new test for solar modulation theory: The 1972 May-July low-energy galactic cosmic-ray proton and helium spectra*, *Astrophys. J.* **182** (1973) L81 .

- [5] D. Hovestadt, O. Vollmer, G. Gloeckler and C.Y. Fan, *Differential Energy Spectra of Low-Energy (<8.5 MeV per Nucleon) Heavy Cosmic Rays during Solar Quiet Times*, *Phys. Rev. Lett.* **31** (1973) 650.
- [6] F.B. McDonald, B.J. Teegarden, J.H. Trainor and W.R. Webber, *The Anomalous Abundance of Cosmic-Ray Nitrogen and Oxygen Nuclei at Low Energies*, *Astrophys. J. Lett.* **187** (1974) L105.
- [7] G. Gloeckler, *Characteristics of solar and heliospheric ion populations observed near earth*, *Advances in Space Research* **4** (1984) 127.
- [8] R.F. Wimmer-Schweingruber and P. Bochsler, *Lunar soils: A long-term archive for the galactic environment of the heliosphere?*, in *Solar and Galactic Composition*, R.F. Wimmer-Schweingruber, ed., (Melville, NY), pp. 399 – 404, AIP conference proceedings, 2001.
- [9] I.G. Usoskin, *A history of solar activity over millennia*, *Living Reviews in Solar Physics* **10** (2013) .
- [10] K.G. McCracken, J. Beer and F.B. McDonald, *The Long-Term Variability of the Cosmic Radiation Intensity at Earth as Recorded by the Cosmogenic Nuclides*, *ISSI Scientific Reports Series* **3** (2005) 83.
- [11] E.W. Cliver, C.J. Schrijver, K. Shibata and I.G. Usoskin, *Extreme solar events*, *Living Reviews in Solar Physics* **19** (2022) 2 [2205.09265].
- [12] E.C. Stone, A.M. Frandsen, R.A. Mewaldt, E.R. Christian, D. Margolies, J.F. Ormes et al., *The Advanced Composition Explorer*, *Space Sci. Rev.* **86** (1998) 1.
- [13] G.M. Mason, R.E. Gold, S.M. Krimigis, J.E. Mazur, G.B. Andrews, K.A. Daley et al., *The Ultra-Low-Energy Isotope Spectrometer (ULEIS) for the ACE spacecraft*, *Space Sci. Rev.* **86** (1998) 409.
- [14] E.C. Stone, C.M.S. Cohen, W.R. Cook, A.C. Cummings, B. Gauld, B. Kecman et al., *The Solar Isotope Spectrometer for the Advanced Composition Explorer*, *Space Sci. Rev.* **86** (1998) 357.
- [15] E.C. Stone, C.M.S. Cohen, W.R. Cook, A.C. Cummings, B. Gauld, B. Kecman et al., *The Cosmic-Ray Isotope Spectrometer for the Advanced Composition Explorer*, *Space Sci. Rev.* **86** (1998) 285.
- [16] D. Müller, O.C. St. Cyr, I. Zouganelis, H.R. Gilbert, R. Marsden, T. Nieves-Chinchilla et al., *The Solar Orbiter mission. Science overview*, *Astron. & Astrophys.* **642** (2020) A1 [2009.00861].
- [17] S.R. Cranmer and A.R. Winebarger, *The Properties of the Solar Corona and Its Connection to the Solar Wind*, *Annual Review of Astronomy & Astrophysics* **57** (2019) 157 [1811.00461].

- [18] O. Witasse, B. Sánchez-Cano, M.L. Mays, P. Kajdič, H. Opgenoorth, H.A. Elliott et al., *Interplanetary coronal mass ejection observed at STEREO-A, Mars, comet 67P/Churyumov-Gerasimenko, Saturn, and New Horizons en route to Pluto: Comparison of its Forbush decreases at 1.4, 3.1, and 9.9 AU*, *Journal of Geophysical Research (Space Physics)* **122** (2017) 7865.
- [19] J.L. Freiherr von Forstner, M. Dumbović, C. Möstl, J. Guo, A. Papaioannou, R. Elftmann et al., *Radial evolution of the April 2020 stealth coronal mass ejection between 0.8 and 1 AU. Comparison of Forbush decreases at Solar Orbiter and near the Earth*, *Astron. & Astrophys.* **656** (2021) A1 [2102.12185].
- [20] M. Desai and J. Giacalone, *Large gradual solar energetic particle events*, *Living Reviews in Solar Physics* **13** (2016) 3.
- [21] A. Brandenburg, *Location of the Solar Dynamo and Near-Surface Shear*, in *Solar MHD Theory and Observations: A High Spatial Resolution Perspective*, J. Leibacher, R.F. Stein and H. Uitenbroek, eds., vol. 354 of *Astronomical Society of the Pacific Conference Series*, p. 121, Dec., 2006 [astro-ph/0512637].
- [22] R.H. Cameron, M. Dikpati and A. Brandenburg, *The Global Solar Dynamo*, *Space Sci. Rev.* **210** (2017) 367 [1602.01754].
- [23] C. García Marirrodriga, A. Pacros, S. Strandmoe, M. Arcioni, A. Arts, C. Ashcroft et al., *Solar Orbiter: Mission and spacecraft design*, *Astron. & Astrophys.* **646** (2021) A121.
- [24] C.J. Owen, R. Bruno, S. Livi, P. Louarn, K. Al Janabi, F. Allegrini et al., *The Solar Orbiter Solar Wind Analyser (SWA) suite*, *Astron. & Astrophys.* **642** (2020) A16.
- [25] T.S. Horbury, H. O'Brien, I. Carrasco Blazquez, M. Bendyk, P. Brown, R. Hudson et al., *The Solar Orbiter magnetometer*, *Astron. & Astrophys.* **642** (2020) A9.
- [26] M. Maksimovic, S.D. Bale, T. Chust, Y. Khotyaintsev, V. Krasnoselskikh, M. Kretschmar et al., *The Solar Orbiter Radio and Plasma Waves (RPW) instrument*, *Astron. & Astrophys.* **642** (2020) A12.
- [27] J. Rodríguez-Pacheco, R.F. Wimmer-Schweingruber, G.M. Mason, G.C. Ho, S. Sánchez-Prieto, M. Prieto et al., *The Energetic Particle Detector. Energetic particle instrument suite for the Solar Orbiter mission*, *Astron. & Astrophys.* **642** (2020) A7.
- [28] R.F. Wimmer-Schweingruber, N.P. Janitzek, D. Pacheco, I. Cernuda, F. Espinosa Lara, R. Gómez-Herrero et al., *First year of energetic particle measurements in the inner heliosphere with Solar Orbiter's Energetic Particle Detector*, *Astron. & Astrophys.* **656** (2021) A22 [2108.02020].
- [29] Rochus, P., Auchère, F., Berghmans, D., Harra, L., Schmutz, W., Schühle, U. et al., *The Solar Orbiter EUI instrument: The Extreme Ultraviolet Imager*, *Astron. & Astrophys.* **642** (2020) A8.

- [30] E. Antonucci, M. Romoli, V. Andretta, S. Fineschi, P. Heinzl, J.D. Moses et al., *Metis: the Solar Orbiter visible light and ultraviolet coronal imager*, *Astron. & Astrophys.* **642** (2020) A10 [1911.08462].
- [31] S.K. Solanki, J.C. del Toro Iniesta, J. Woch, A. Gandorfer, J. Hirzberger, A. Alvarez-Herrero et al., *The Polarimetric and Helioseismic Imager on Solar Orbiter*, *Astron. & Astrophys.* **642** (2020) A11 [1903.11061].
- [32] SPICE Consortium, M. Anderson, T. Appourchaux, F. Auchère, R. Aznar Cuadrado, J. Barbay et al., *The Solar Orbiter SPICE instrument. An extreme UV imaging spectrometer*, *Astron. & Astrophys.* **642** (2020) A14 [1909.01183].
- [33] Howard, R. A., Vourlidas, A., Colaninno, R. C., Korendyke, C. M., Plunkett, S. P., Carter, M. T. et al., *The solar orbiter heliospheric imager (solohi)*, *Astron. & Astrophys.* **642** (2020) A13.
- [34] L. Wang, R.P. Lin, S. Krucker and G.M. Mason, *A Statistical Study of Solar Electron Events over One Solar Cycle*, *Astrophys. J.* **759** (2012) 69.
- [35] R. Gómez-Herrero, D. Pacheco, A. Kollhoff, F. Espinosa Lara, J.L. Freiherr von Forstner, N. Dresing et al., *First near-relativistic solar electron events observed by EPD onboard Solar Orbiter*, *Astron. & Astrophys.* **656** (2021) L3.
- [36] W. Wang, L. Wang, S. Krucker, G.M. Mason, Y. Su and R. Bučík, *Solar Energetic Electron Events Associated with Hard X-Ray Flares*, *Astrophys. J.* **913** (2021) 89.
- [37] G.M. Mason, G.C. Ho, R.C. Allen, J. Rodríguez-Pacheco, R.F. Wimmer-Schweingruber, R. Bučík et al., *³He-rich solar energetic particle events observed on the first perihelion pass of Solar Orbiter*, *Astron. & Astrophys.* **656** (2021) L1.
- [38] L. Wang, R.P. Lin and S. Krucker, *Pitch-angle Distributions and Temporal Variations of 0.3-300 keV Solar Impulsive Electron Events*, *Astrophys. J.* **727** (2011) 121.
- [39] Y.M. Wang, M. Pick and G.M. Mason, *Coronal Holes, Jets, and the Origin of ³He-rich Particle Events*, *Astrophys. J.* **639** (2006) 495.
- [40] N.V. Nitta, G.M. Mason, M.E. Wiedenbeck, C.M.S. Cohen, S. Krucker, I.G. Hannah et al., *Coronal Jet Observed by Hinode as the Source of a ³He-rich Solar Energetic Particle Event*, *Astrophys. J. Lett.* **675** (2008) L125.
- [41] R. Bučík, M.E. Wiedenbeck, G.M. Mason, R. Gómez-Herrero, N.V. Nitta and L. Wang, *³He-rich Solar Energetic Particles from Sunspot Jets*, *astrophys. J. Lett.* **869** (2018) L21 [1812.07735].
- [42] R. Bučík, G.M. Mason, R. Gómez-Herrero, D. Lario, L. Balmaceda, N.V. Nitta et al., *The long period of ³He-rich solar energetic particles measured by Solar Orbiter 2020 November 17-23*, *Astron. & Astrophys.* **656** (2021) L11 [2109.05570].

- [43] G.M. Mason, C.M.S. Cohen, G.C. Ho, D.G. Mitchell, R.C. Allen, M.E. Hill et al., *Solar energetic particle heavy ion properties in the widespread event of 2020 November 29*, *Astron. & Astrophys.* **656** (2021) L12.
- [44] D. Band, J. Matteson, L. Ford, B. Schaefer, D. Palmer, B. Teegarden et al., *BATSE Observations of Gamma-Ray Burst Spectra. I. Spectral Diversity*, *Astrophys. J.* **413** (1993) 281.
- [45] M.I. Desai, G.M. Mason, R.E. Gold, S.M. Krimigis, C.M.S. Cohen, R.A. Mewaldt et al., *Heavy-Ion Elemental Abundances in Large Solar Energetic Particle Events and Their Implications for the Seed Population*, *Astrophys. J.* **649** (2006) 470.
- [46] C.M.S. Cohen, E.R. Christian, A.C. Cummings, A.J. Davis, M.I. Desai, G.A. de Nolfo et al., *PSP/IS \odot IS observations of the 29 November 2020 solar energetic particle event*, *Astron. & Astrophys.* **656** (2021) A29.
- [47] H.V. Cane, R.A. Mewaldt, C.M.S. Cohen and T.T. von Roseninge, *Role of flares and shocks in determining solar energetic particle abundances*, *J. Geophys. Res. (Space Phys.)* **111** (2006) A06S90.
- [48] M.I. Desai, G.M. Mason, J.E. Mazur and J.R. Dwyer, *The Seed Population for Energetic Particles Accelerated by CME-Driven Shocks*, *Space Sci. Rev.* **124** (2006) 261.
- [49] A. Kollhoff, A. Kouloumvakos, D. Lario, N. Dresing, R. Gómez-Herrero, L. Rodríguez-García et al., *The first widespread solar energetic particle event observed by Solar Orbiter on 2020 November 29*, *Astron. & Astrophys.* **656** (2021) A20.
- [50] G.M. Mason, G.C. Ho, R.C. Allen, Z.G. Xu, N.P. Janitzek, J.L. Freiherr von Forstner et al., *Quiet-time low energy ion spectra observed on Solar Orbiter during solar minimum*, *Astron. & Astrophys.* **656** (2021) L5.
- [51] R.A. Mewaldt, A.C. Cummings, J.R. Cummings, E.C. Stone, B. Klecker, D. Hovestadt et al., *The return of the anomalous cosmic rays to 1 AU in 1992*, *Geophys. Res. Lett.* **20** (1993) 2263.
- [52] R.C. Allen, G.M. Mason, G.C. Ho, J. Rodríguez-Pacheco, R.F. Wimmer-Schweingruber, G.B. Andrews et al., *Suprathermal particles from corotating interaction regions during the first perihelion pass of Solar Orbiter*, *Astron. & Astrophys.* **656** (2021) L2.
- [53] D. Telloni, L. Sorriso-Valvo, L.D. Woodham, O. Panasenco, M. Velli, F. Carbone et al., *Evolution of Solar Wind Turbulence from 0.1 to 1 au during the First Parker Solar Probe-Solar Orbiter Radial Alignment*, *Astrophys. J. Lett.* **912** (2021) L21.
- [54] D. Telloni, V. Andretta, E. Antonucci, A. Bemporad, G.E. Capuano, S. Fineschi et al., *Exploring the Solar Wind from Its Source on the Corona into the Inner Heliosphere during the First Solar Orbiter-Parker Solar Probe Quadrature*, *Astrophys. J. Lett.* **920** (2021) L14 [2110.11031].

- [55] L. Adhikari, G.P. Zank, L.L. Zhao, D. Telloni, T.S. Horbury, H. O'Brien et al., *Evolution of anisotropic turbulence in the fast and slow solar wind: Theory and Solar Orbiter measurements*, *Stron. & Astrophys.* **656** (2021) A6.
- [56] S.E. Forbush, *On the Effects in Cosmic-Ray Intensity Observed During the Recent Magnetic Storm*, *Physical Review* **51** (1937) 1108.
- [57] E.K.J. Kilpua, S.W. Good, N. Dresing, R. Vainio, E.E. Davies, R.J. Forsyth et al., *Multi-spacecraft observations of the structure of the sheath of an interplanetary coronal mass ejection and related energetic ion enhancement*, *Astron. & Astrophys.* **656** (2021) A8 [2112.09472].
- [58] H.E. Spence, A.W. Case, M.J. Golightly, T. Heine, B.A. Larsen, J.B. Blake et al., *CRaTER: The Cosmic Ray Telescope for the Effects of Radiation Experiment on the Lunar Reconnaissance Orbiter Mission*, *Space Sci. Rev.* **150** (2010) 243.
- [59] C.R. Tooley, M.B. Houghton, R.S. Saylor, C. Peddie, D.F. Everett, C.L. Baker et al., *Lunar Reconnaissance Orbiter Mission and Spacecraft Design*, *Space Sci. Rev.* **150** (2010) 23.
- [60] J. O'Kane, L.M. Green, E.E. Davies, C. Möstl, J. Hinterreiter, J.L. Freiherr von Forstner et al., *Solar origins of a strong stealth CME detected by Solar Orbiter*, *Astron. & Astrophys.* **656** (2021) L6 [2103.17225].
- [61] E.E. Davies, C. Möstl, M.J. Owens, A.J. Weiss, T. Amerstorfer, J. Hinterreiter et al., *In situ multi-spacecraft and remote imaging observations of the first CME detected by Solar Orbiter and BepiColombo*, *Astron. & Astrophys.* **656** (2021) A2 [2012.07456].
- [62] L.L. Zhao, G.P. Zank, J.S. He, D. Telloni, Q. Hu, G. Li et al., *Turbulence and wave transmission at an ICME-driven shock observed by the Solar Orbiter and Wind*, *Astron. & Astrophys.* **656** (2021) A3 [2102.03301].
- [63] N.J. Fox, M.C. Velli, S.D. Bale, R. Decker, A. Driesman, R.A. Howard et al., *The Solar Probe Plus Mission: Humanity's First Visit to Our Star*, *Space Sci. Rev.* **204** (2016) 7.
- [64] M.L. Kaiser, T.A. Kucera, J.M. Davila, O.C. St. Cyr, M. Guhathakurta and E. Christian, *The STEREO Mission: An Introduction*, *Space Science Reviews* **136** (2008) 5.
- [65] H. Kunow, M.A. Lee, L.A. Fisk, R.J. Forsyth, B. Heber, T.S. Horbury et al., *Corotating Interaction Regions at High Latitudes*, in *Corotating Interaction Regions. Series: Space Sciences Series of ISSI*, A. Balogh, J.T. Gosling, J.R. Jokipii, R. Kallenbach and H. Kunow, eds., vol. 7, pp. 221–268 (1999), DOI.
- [66] L.A. Fisk and M.A. Lee, *Shock acceleration of energetic particles in corotating interaction regions in the solar wind*, *Astrophys. J.* **237** (1980) 620 .
- [67] M.A.I. Van Hollebeke, F.B. McDonald, J.H. Trainor and T.T. von Roseninge, *The radial variation of corotating energetic particle streams in the inner and outer solar system*, *J. Geophys. Res.* **83** (1978) 4723.

- [68] S.P. Christon and J.A. Simpson, *Separation of corotating nucleon fluxes from solar flare fluxes by radial gradients and nuclear composition.*, *Astrophys. J. Lett.* **227** (1979) L49.
- [69] A. Aran, D. Pacheco, M. Laurenza, N. Wijsen, D. Lario, S. Benella et al., *Evidence for local particle acceleration in the first recurrent galactic cosmic ray depression observed by Solar Orbiter. The ion event on 19 June 2020*, *Astron. & Astrophys.* **656** (2021) L10.
- [70] G.M. Mason, *Composition and energy spectra of ions accelerated in Corotating Interaction Regions*, in *Acceleration and Transport of Energetic Particles Observed in the Heliosphere*, R.A. Mewaldt, J.R. Jokipii, M.A. Lee, E. Möbius and T.H. Zurbuchen, eds., vol. 528 of *American Institute of Physics Conference Series*, pp. 234–241, Sept., 2000, DOI.
- [71] J. Giacalone, J.R. Jokipii and J. Kóta, *Particle Acceleration in Solar Wind Compression Regions*, *Astrophys. J.* **573** (2002) 845.
- [72] R.C. Allen, I. Cernuda, D. Pacheco, L. Berger, Z.G. Xu, J.L. Freiherr von Forstner et al., *Energetic ions in the Venusian system: Insights from the first Solar Orbiter flyby*, *Astron. & Astrophys.* **656** (2021) A7.
- [73] A.P. Dimmock, Y.V. Khotyaintsev, A. Lalti, E. Yordanova, N.J.T. Edberg, K. Steinvall et al., *Analysis of multiscale structures at the quasi-perpendicular Venus bow shock. Results from Solar Orbiter’s first Venus flyby*, *Astron. & Astrophys.* **660** (2022) A64.
- [74] L.Z. Hadid, N.J.T. Edberg, T. Chust, D. Pířa, A.P. Dimmock, M.W. Morooka et al., *Solar Orbiter’s first Venus flyby: Observations from the Radio and Plasma Wave instrument*, *Astron. & Astrophys.* **656** (2021) A18.
- [75] M. Volwerk, T.S. Horbury, L.D. Woodham, S.D. Bale, C. Simon Wedlund, D. Schmid et al., *Solar Orbiter’s first Venus flyby. MAG observations of structures and waves associated with the induced Venusian magnetosphere*, *Astron. & Astrophys.* **656** (2021) A11.
- [76] D. Berghmans, F. Auchère, D.M. Long, E. Soubrié, M. Mierla, A.N. Zhukov et al., *Extreme-UV quiet Sun brightenings observed by the Solar Orbiter/EUI*, *Astron. & Astrophys.* **656** (2021) L4 [2104.03382].